Chapter 8
Handheld NMR Systems and Their Applications for Biomolecular Sensing

Nan Sun and Donhee Ham

Abstract We have developed a miniature nuclear magnetic resonance (NMR) system. By combining the physics of NMR with CMOS radio-frequency ICs, we developed a 0.1-kg palm NMR system that is 1,200 times smaller, 1,200 times lighter, and yet 150 times more spin-mass sensitive than a state-of-the-art 120-kg commercial benchtop system. The small NMR system can be used for disease detection and medical diagnostics. It was demonstrated capable of detecting human cancer cells and cancer marker proteins.

8.1 Introduction

Nuclear magnetic resonance (NMR) is the energy exchange between a radio-frequency (RF)-varying magnetic field and an atomic nucleus such as a hydrogen proton, which acts like a tiny bar magnet due to its spin. Since the detailed resonance behavior is influenced by the environment of the nucleic magnets, NMR can be used to examine properties of a material, and thus, it has a wide array of applications in technology and science, such as biomolecular sensing, medical imaging, and oil detection, just to name a few.

The benefits of NMR would be broadly available, if NMR instruments can be made small, thus, at low cost. For example, a miniature NMR biosensor may enable disease screening in a doctor's office or a patient's home at an affordable

N. Sun
Department of Electrical and Computer Engineering, University of Texas at Austin, Austin TX USA
e-mail: nansun@mail.utexas.edu

D. Ham (✉)
School of Engineering and Applied Sciences, Harvard University, Cambridge MA USA
e-mail: donhee@seas.harvard.edu

D. Issadore and R.M. Westervelt (eds.), *Point-of-Care Diagnostics on a Chip*,
Biological and Medical Physics, Biomedical Engineering,
DOI 10.1007/978-3-642-29268-2_8, © Springer-Verlag Berlin Heidelberg 2013

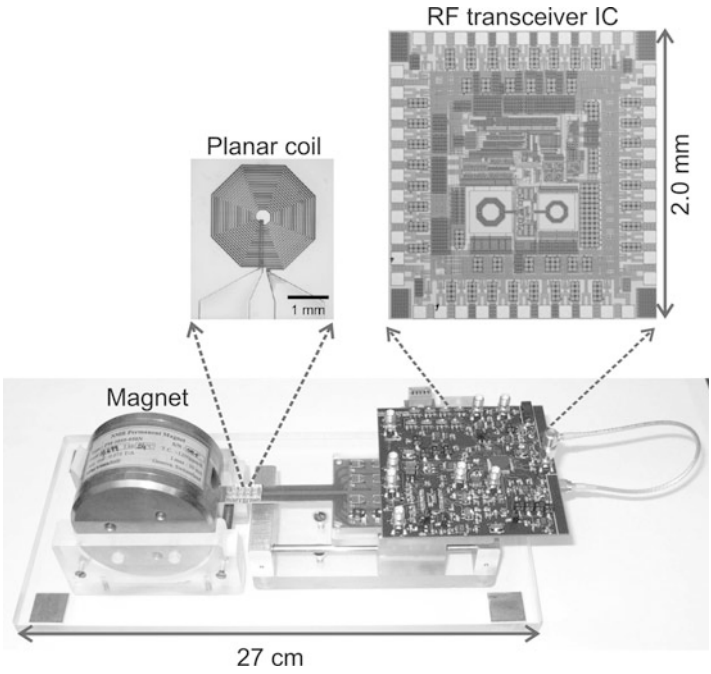

Fig. 8.1 2-kg portable NMR system (From Ref. [2])

cost. Nonetheless, NMR systems remain bulky, heavy, and expensive, with their use limited in hospitals, testing facilities, and laboratories. A case in point is the state-of-the-art commercial benchtop NMR system of [1], which weighs approximately 120 kg.

The large size is due to the following reason. An NMR system consists of a magnet to produce a static magnetic field, a sample coil, and an RF transceiver to generate an RF magnetic field and to monitor the resonance. Since a larger-sized magnet tends to yield a stronger NMR signal even for the same static magnetic field strength and hence relaxes the sensitivity requirement on the transceiver design, large magnets are used, leading to the bulky size, where the magnet is by far the largest component.

To miniaturize an NMR system, we took an approach opposite to the convention: we chose to use small magnets, and to detect the NMR signal substantially weakened by the small magnets, we developed highly sensitive RF transceivers. Furthermore, we integrated the RF transceiver onto silicon integrated circuit (IC) chips. As small magnets are used, the transceiver integration makes sense: in a conventional system where a large and expensive magnet dominates the system size and cost, integration of the RF transceiver would hardly reduce either the system size or the cost.

Our efforts first led to the construction of a *portable NMR system* shown in Fig. 8.1 [2]. Occupying only 2.5 L and weighing only 2 kg, this system is 60 times lighter, 40 times smaller, yet 60 times more spin-mass sensitive than the state-of-the-art benchtop NMR system of [1]. It uses a small magnet, the size of a hamburger

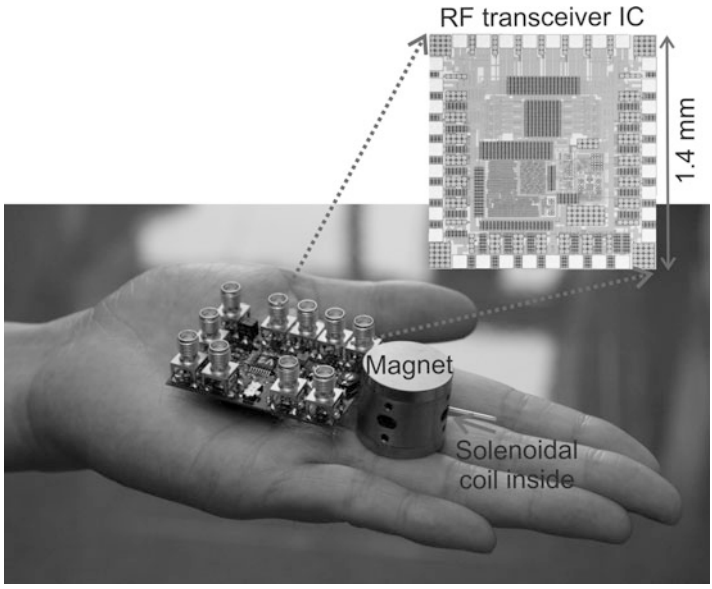

Fig. 8.2 0.1-kg palm NMR system (From Ref. [3])

(this magnet and the magnet of the commercial system both produce the static field of approximately 0.5 T). To receive the NMR signal weakened by the small magnet, we developed a partially integrated, high-performance RF transceiver and a separate high-quality planar coil.

After the design of the 2-kg portable system, we developed two new miniature NMR systems, which we call *the palm NMR system* and the *1-chip NMR system* [3]. They represent yet another orders-of-magnitude size reduction and lab-on-a-chip capability. The palm NMR system, shown in Fig. 8.2, is the smallest complete NMR system to our best knowledge. It is 1,200 times lighter, 1,200 times smaller, yet 150 times more spin-mass sensitive than the 120-kg commercial system of [1]. As compared to the 2-kg portable NMR system, the palm system is 20 times lighter, 30 times smaller, and yet 2.5 times more spin-mass sensitive. To attain this further substantial size and cost reduction, we use a tiny magnet only the size of a ping-pong ball. This considerably lowers the NMR signal, which we overcome by designing a new, high-performance RF transceiver. As the signal is already lowered by the ping-pong-ball-sized magnet, the palm system uses a high-quality solenoidal coil, not to further weaken the signal.

The 1-chip NMR system is shown in Fig. 8.3. In this system, even the NMR coil is integrated as a planar spiral in the silicon IC chip along with the transceiver developed for the palm system. The transceiver's performance allows the use of the lossy on-chip coil that lowers the signal-to-noise ratio. Not to further weaken the signal-to-noise ratio, the 1-chip system operates with the same hamburger-sized magnet of the 2-kg portable system. Due to this magnet, the weight reduction from the portable system is by 25 %, but the point of the 1-chip system is lab-on-a-chip

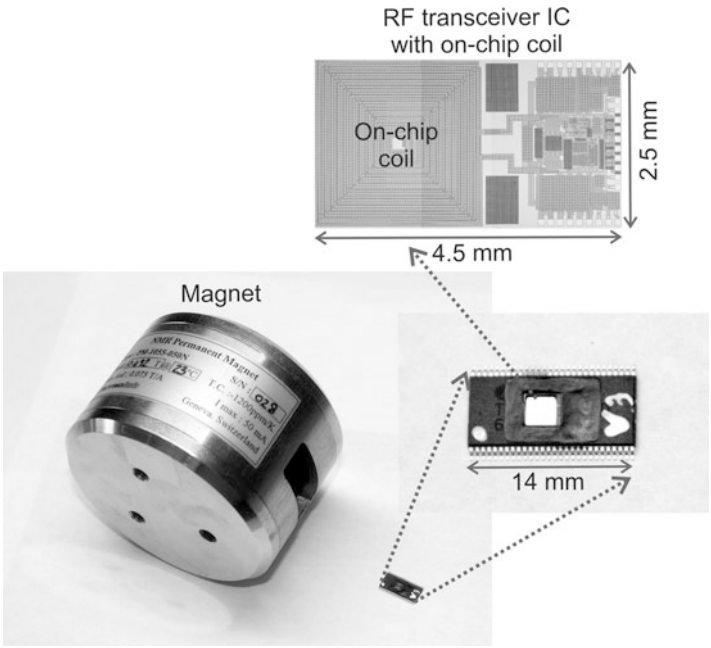

Fig. 8.3 1-chip NMR system with lab-on-a-chip capability (From Ref. [3])

operation. For example, a biological sample can be placed directly on the coil of the chip for on-chip screening of disease markers. The chip can be disposable for one-time diagnostic testing. The direct interface may also enable oil detection [4] and quantum computing [5] on a silicon chip. The 1-chip system has the same spin-mass sensitivity as the 2-kg portable system while 60 times more spin-mass sensitive than the commercial system of [1].

The key to these two new developments is the new RF transceiver, an advance from the transceiver in the 2-kg portable system. First, the new transceiver achieves the sensitivity to cope with the signal-to-noise ratio lowered by the ping-pong-ball-sized magnet (palm system) or the lossy on-chip coil (1-chip system). Second, the new transceiver attains the highest level of integration among existing NMR transceivers. The transceiver in the 2-kg portable system did not integrate a power amplifier (PA), as meeting the large power tuning requirement of NMR was nontrivial with an integrated PA. We integrate a PA in the new transceiver by devising a power tuning scheme that exploits the natural high-Q ($\sim 10^4$) filtering ability of atomic nuclei.

We used our three miniature NMR systems to detect various kinds of biomolecules relevant to disease screening. For example, we detected avidin, folic acid, and human chorionic gonadotropin (hCG), which can be used as a cancer marker for male patients for cancers such as choriocarcinoma, germ cell tumor, and islet cell tumor. At the cell level, we detected human bladder cancer cells.

This chapter explains the construction and experiment of our miniature NMR systems. Its organization is as follows. Sections 8.2 and 8.3 present the design and measurement of the silicon RF transceivers. Section 8.4 reports NMR experiments and NMR-based biomolecular sensing. Section 8.5 compares our miniature NMR systems to other NMR miniaturization efforts. We recommend readers unfamiliar with NMR to read our publication of [2] for quick introduction to NMR basics relevant to our work.

8.2 NMR RF Transceiver IC Design

8.2.1 Overall Architecture and Operation

We focus our discussion on the transceivers in the palm and 1-chip systems (Figs. 8.2 and 8.3), for they are more advanced than the transceiver in the 2-kg portable system (Fig. 8.1). Figure 8.4a and b shows the architectures of the NMR RF transceivers in the palm and 1-chip systems, respectively. The palm system (Fig. 8.4a) uses an off-chip solenoidal coil; the 1-chip system (Fig. 8.4b) employs an on-chip planar spiral coil. The dashed lines in the figures indicate silicon integration boundaries for the two systems. The transceiver architecture is essentially the same between the two systems, but the transceiver-coil matching networks are different for a reason explained in Sect. 8.2.4; thus, the two separate figures were prepared to avoid confusion. The electrical characteristics of the coils will be described in Sect. 8.2.4. All NMR experiments in our work, including biomolecular sensing, are done with protons in hydrogen atoms in aqueous samples. In the palm system, a sample is placed inside the solenoidal coil and is subjected to a static magnetic field B_0 of 0.56 T produced by the ping-pong-ball-sized magnet. In the 1-chip system, a sample placed on the planar coil is subjected to a static magnetic field B_0 of 0.49 T produced by the hamburger-sized magnet. The NMR frequency for protons subjected to is given by $\omega_0/2\pi = 42.6 \cdot B_0$ MHz: 23.9 MHz for the palm system and 20.9 MHz for the 1-chip system.

In the excitation phase of NMR, switches S1 and S2 are closed, and the transmitter (upper half of Fig. 8.4a or b) sends in an RF current to the coil to produce an RF magnetic field in the sample. If the RF magnetic field's frequency is tuned into the NMR frequency, ω_0, it resonantly excites the protons, increasing their energy. During this excitation phase, the receiver amplifier stages (in the lower half of Fig. 8.4a or b), except the front-end stage, are isolated from the large excitation signal by short-circuiting their inputs and open-circuiting the RF signal path, using switches S3 through S11 controlled by the ENA command signal. The front-end stage remains connected to the large excitation signal, in order not to place switches in front of it, as lossy switches at the front end would compromise the receiver noise figure.

After protons acquire sufficient energy, the RF transmission is ceased by turning off switches S1 and S2. Nearly simultaneously, the receiver path (lower half of

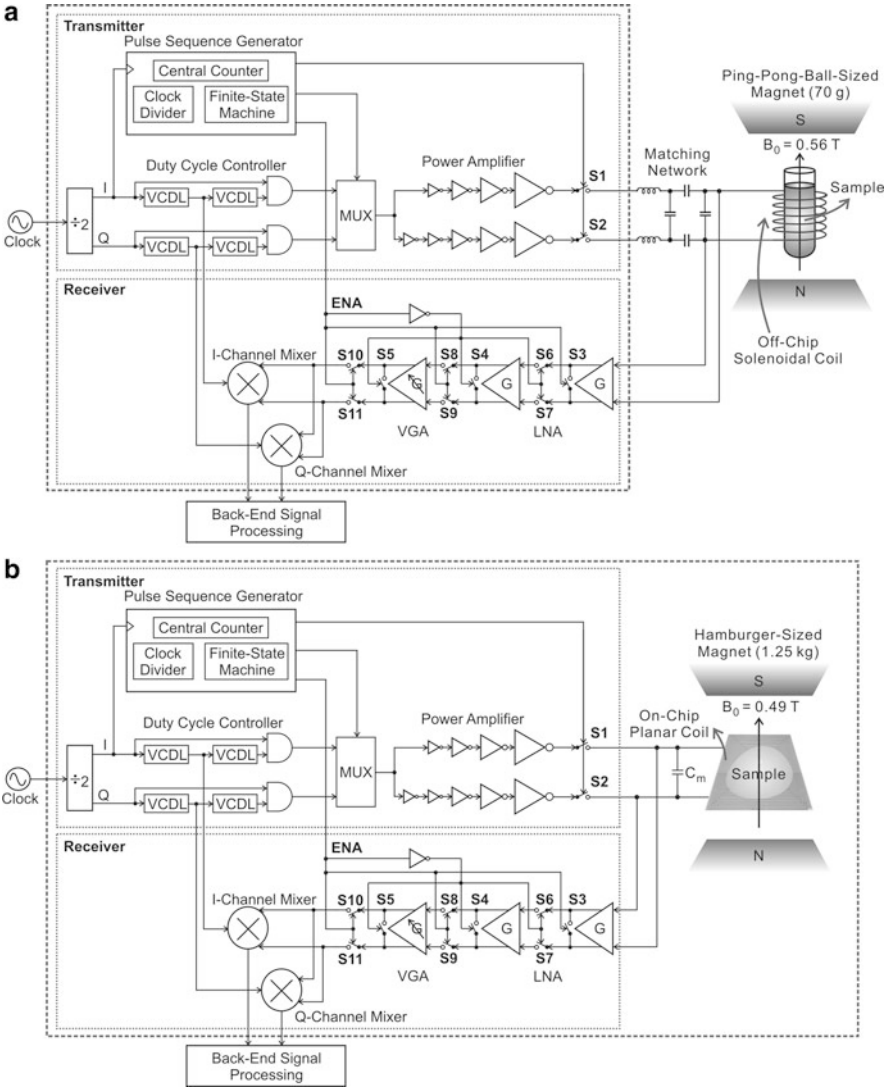

Fig. 8.4 NMR RF transceiver architectures for (**a**) the palm system and (**b**) the 1-chip system (From Ref. [3])

Fig. 8.4a or b) is activated by operating switches S3 through S11 in the configuration that is opposite to their configuration during the excitation phase. In this reception phase of NMR, the excited protons electromagnetically interact with the coil, inducing an AC voltage signal with the NMR frequency, ω_0, across the coil. This NMR signal, whose peak-to-peak voltage is on the order of 100 nV and bandwidth is about 1 kHz, is amplified and frequency down-converted by the heterodyne receiver. The intermediate frequency (IF) for the receiver is set at 3 kHz, which is high

enough to mitigate the $1/f$ noise and low enough to facilitate the rejection of out-of-band noise by placing an off-chip band-pass filter at the outputs of the mixers. Two mixers are used to perform the frequency down-conversion with quadrature oscillator outputs. The outputs of the mixers, after the band-pass filtering, are digitized by an off-chip analog-to-digital converter and subsequently undergo an image rejection signal processing, to avoid the extra 3-dB noise figure degradation brought by the frequency down-conversion.

NMR transceivers usually employ two separate clocks, one with the NMR frequency for the proton excitation and the other as the local oscillator (LO) with the frequency different than the NMR frequency by the target IF to produce the correct IF. In contrast, in our transceiver, both the transmitter excitation signal and the receiver local oscillator signal share the identical frequency, both derived from the same clock (Fig. 8.4). In this scheme the clock frequency is set at a value 3 kHz larger than the NMR frequency ω_0 so as to produce the target IF of 3 kHz. Therefore, the excitation signal is 3 kHz off from the NMR frequency. Nonetheless, it can still excite protons, for it has a nonzero bandwidth due to its finite duration and the bandwidth can be made large enough to cover ω_0. The advantage of this single-clock scheme is simplicity: we only need to tune one frequency in the NMR experiment, instead of tuning two clock frequencies while maintaining their difference at 3 kHz.

8.2.2 Characteristics of the Coils

The off-chip solenoidal coil of the palm system (Figs. 8.2 and 8.4a) has 14 turns around a capillary tube (inner diameter, 0.75 mm; outer diameter, 1 mm). The sample volume inside the coil is 2 μL. The coil has an inductance of 100 nH, a resistance of 0.5Ω, and a Q of 28, all measured at the NMR frequency 23.9 MHz of the palm system.

The on-chip planar spiral coil of the 1-chip system (Figs. 8.3 and 8.4b) has 25 turns and occupies an area of 2.5 by 2.5 mm. We use a package that exposes the coil part while encapsulating the rest of the chip (Fig. 8.3). The open part of the package above the coil can hold a 5 μL of sample. To reduce the coil resistance, five metal layers are connected in parallel. SONNET electromagnetic field solver is used in the coil design. The coil has an inductance of 430 nH, a resistance of 31Ω, and a Q of 1.9, all measured at the NMR frequency 20.9 MHz of the 1-chip system. The low Q is due mainly to the coil's dc resistance, while the substrate and skin effect are less pronounced at the NMR frequency.

8.2.3 Transmitter with Proton Filter

The power amplifier (PA) of the NMR transmitter in general needs to have a large output power tuning capability in order to control the amount of energy

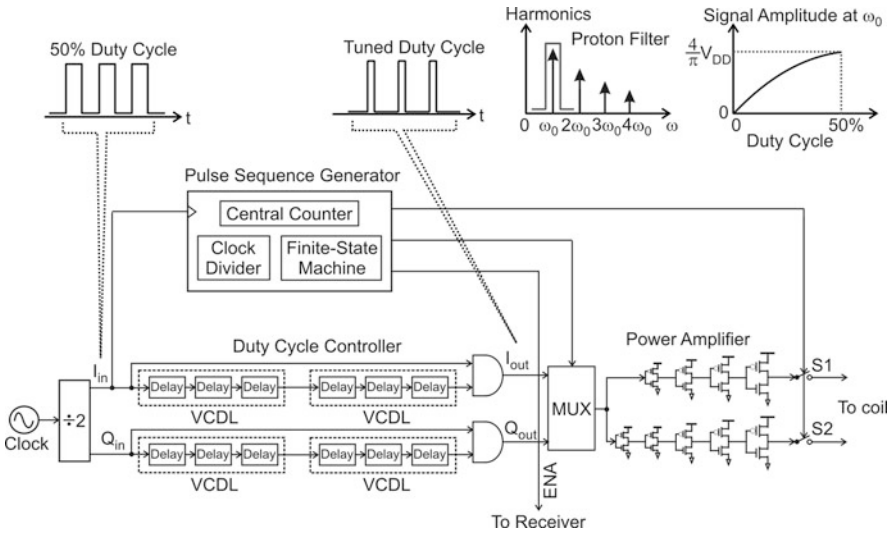

Fig. 8.5 Transmitter chain and power tuning scheme (From Ref. [3])

that goes into the protons during the NMR excitation phase. The transmitter in the 2-kg portable system did not integrate a PA, since meeting the power tuning requirement was not trivial with an integrated PA. The new transmitter in the palm and 1-chip systems, which is shown in detail in Fig. 8.5, integrates the entire front-end transmitter chain, including a PA. We manage to tune the PA's output power by exploiting the proton's natural high-Q ($\sim 10^4$) filtering ability.

To start with, the PA is realized as a differential chain of cascaded four inverter stages (Fig. 8.5, bottom right). The inverters are consecutively quadrupled in size to sequentially amplify power and ensure drivability at the output. This class-D arrangement is simple to design and does not consume static power, but it produces a square wave output with fixed voltage amplitude of the power supply V_{DD}, thus, calling for a technique to tune its output power.

To this end, we tune the duty cycle of the transmitted signal. A given transmitted square wave (frequency: ω_0; amplitude: V_{DD}) with a specific duty cycle (Fig. 8.5, top) assumes a particular power distribution of the fundamental tone at ω_0 and higher-order harmonics. The power distribution over the harmonics varies with the duty cycle. Here we only need to look at the variation of the power at ω_0 with the duty cycle, for higher-order harmonics lie outside the "proton filter" band: protons are a high-Q ($\sim 10^4$) band-pass filter centered at ω_0, in the sense that they are not excited by signals that lie outside the frequency band. As the duty cycle is altered from 0 % to 50 %, the ω_0-component changes its voltage from 0 to $(4/\pi)\ \ V_{DD}$ (Fig. 8.5, top right). This effectively corresponds to the output power tuning.

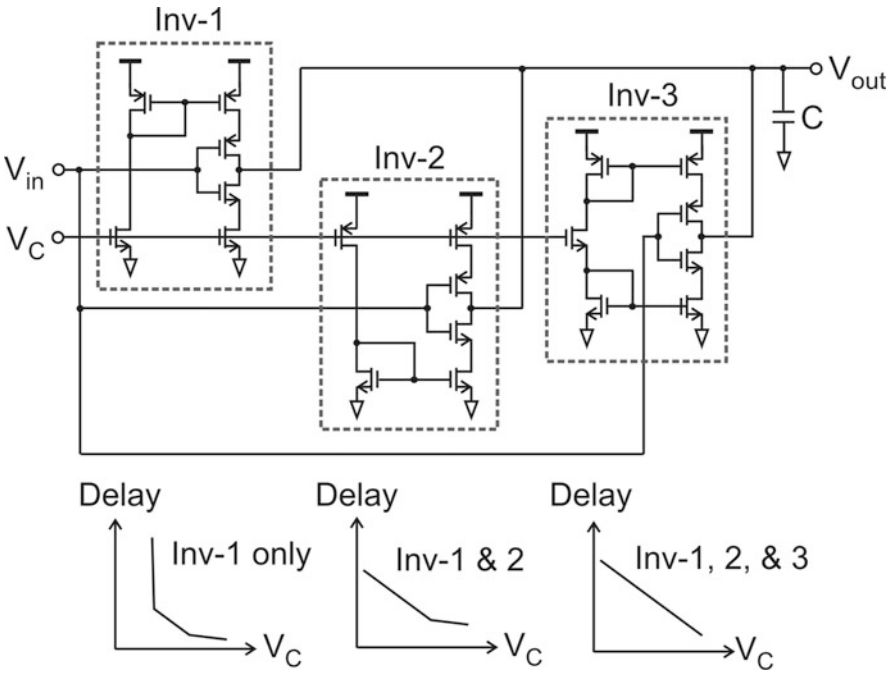

Fig. 8.6 Schematic of a single delay cell

The duty cycle is tuned by the duty cycle controller that consists of cascaded voltage-controlled delay lines (VCDL) and AND gates (Fig. 8.5, bottom left). Both of its quadrature square-wave inputs, I_{in} and Q_{in} (frequency: ω_0; amplitude: V_{DD}), have a 50 % duty cycle. The AND operation on I_{in} and its delayed version yields I_{out}, whose duty cycle varies with the amount of the total delay. The same principle applies to Q_{in} and Q_{out}. As the total delay changes from 0 to π/ω_0, the duty cycle shifts from 50 % to 0 %.

Each voltage-controlled delay line in the duty cycle controller consists of three voltage-controlled delay cells, and each voltage-controlled delay cell consists of three voltage-controlled inverters in parallel (Fig. 8.6). Inv-1 is a standard current-starved inverter. Its delay is not linear with control voltage V_C: with V_C below a certain threshold, the delay tends toward infinity; with large V_C, the delay hardly tunes. Inv-2, a complementary current-starved inverter with a size smaller than Inv-1, prevents the steep delay increase for small V_C. Inv-3, a current-starved inverter with V_C fed after a source follower, sustains a delay reduction with increasing V_C. These combine together to yield a more linear tuning characteristics.

The digital pulse sequence generator (Fig. 8.5, upper left) controls the MUX and switches S1 and S2 to produce an adequate NMR excitation pulse sequence such as the CPMG pulse sequence, an essential task in practical NMR works [6]. The

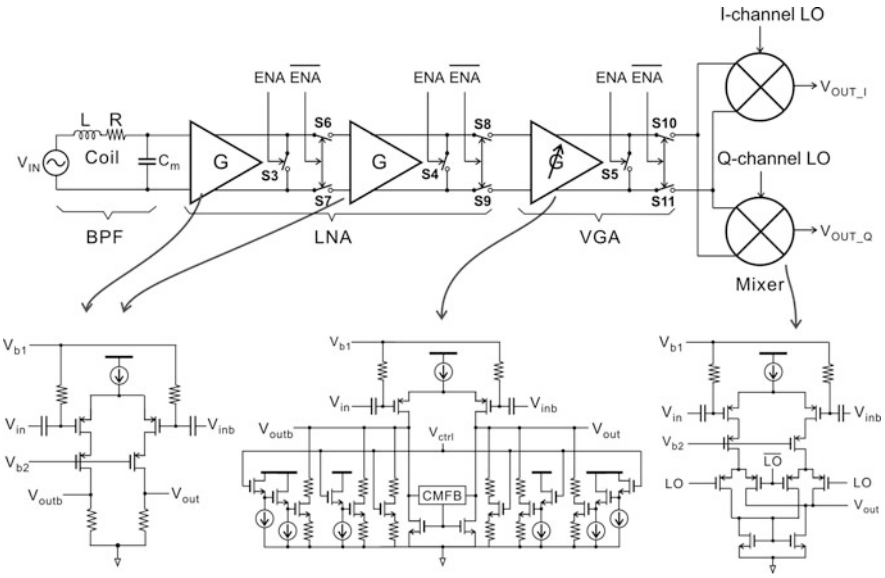

Fig. 8.7 Receiver chain (From Ref. [3])

pulse sequence generator also sets the timing scheme for the receiver by controlling switches S3 through S11 (see also Fig. 8.4) in the way explained in Sect. 8.2.1.

8.2.4 Heterodyne Receiver with Passive Amplification

Figure 8.7 shows the detailed structure of the heterodyne receiver, which consists of a low-noise amplifier (LNA), a variable-gain amplifier (VGA), two mixers, and switches S3 through S11, whose usage was explained in Sect. 8.2.1. To handle the NMR signal-to-noise ratio substantially lowered by the ping-pong-ball-sized magnet in the palm system or the lossy on-chip coil in the 1-chip system, the noise figure (NF) of the receiver should be minimized. To this end, both minimization of the LNA's input-referred noise and optimum LNA-coil noise matching are necessary.

To minimize the LNA's input-referred noise, we take the following measures in our new LNA design: (1) resistive loads are used in place of active loads. This obviates the need for a common-mode feedback circuit, thus reducing the noise sources. To compensate for the low gain due to the passive loads, we use a two-stage amplifier; (2) PMOS transistors are used as input devices to minimize $1/f$ noise and substrate coupling from digital circuits; and (3) the cascode configuration attenuates coupling between the local oscillator and the LNA. For the optimum LNA-coil noise

matching, we place a capacitor C_m in parallel with the coil (Fig. 8.7, left), where C_m resonates with the coil inductance at the NMR frequency ω_0. This network forms a band-pass filter, whose frequency response peaks at ω_0. The filter may be viewed as a preamplifier with "passive" voltage gain of Q, where Q is the coil quality. As C_m has negligible loss compared to the coil, the passive amplification hardly adds any noise and maintains the original signal-to-noise ratio from the coil. In other words, the passive amplifier has an NF close to 0 dB but with the gain of Q, which leads to a low receiver NF according to the Friis equation [7]. While this passive amplification scheme is not applicable for wideband signals due to the frequency-dependent transfer function, it suits well the NMR signal, which in general has a very narrow bandwidth (about 1 kHz in our case). Nonetheless, nonoptimal coil-LNA impedance matching at 50Ω, instead of the optimum noise matching based on the passive amplification, has been a conventional choice, as the former is convenient in the conventional NMR electronics that have largely been realized at the discrete level. This shows an advantage of the integrated NMR electronics.

The LNA-coil resonance matching for minimum noise figure corresponds to an impedance mismatch between the LNA and the coil. In contrast, the PA and the coil need to be impedance matched for maximum power delivery. In order to simultaneously achieve both the optimum LNA-coil noise matching and PA-coil power matching, the palm system adopts an advanced matching network (Fig. 8.4a, right). In the 1-chip system, on the other hand, we provide only the LNA-coil resonance matching using C_m (Fig. 8.4b, right) without using the advanced network; thus, the PA and the coil are not impedance matched. This is because the components of the advanced network are too large to be integrated, and using discrete components defeats the purpose of constructing a 1-chip system. Nonetheless, the 1-chip system manages to deliver a reasonable amount of power to the coil for proton excitation.

The VGA (Fig. 8.7) is to handle both the palm and 1-chip systems, whose NMR signal strengths are different. It is a differential common-source amplifier with tunable loads. By tuning the load impedance through V_{ctrl}, we can change the gain of the VGA from 0.8 to 22. The mixer is a double-balanced Gilbert mixer with an active load. It provides a voltage gain of 26 dB.

8.3 Transceiver Measurements

We implemented two variations of the NMR RF transceiver with essentially the same architecture (Fig. 8.4), one for the palm system and the other for the 1-chip system, in 0.18-μm complementary-metal-oxide-semiconductor (CMOS) technology. The transceiver IC for the palm system occupies an area of 1.4 by 1.4 mm (Fig. 8.2) and is packaged in a 32-lead QFP package. The transceiver IC with the on-chip planar coil for the 1-chip system occupies an area of 4.5 by 2.5 mm (Fig. 8.3) and is so packaged in a 56-lead TSSOP package that the coil part of the

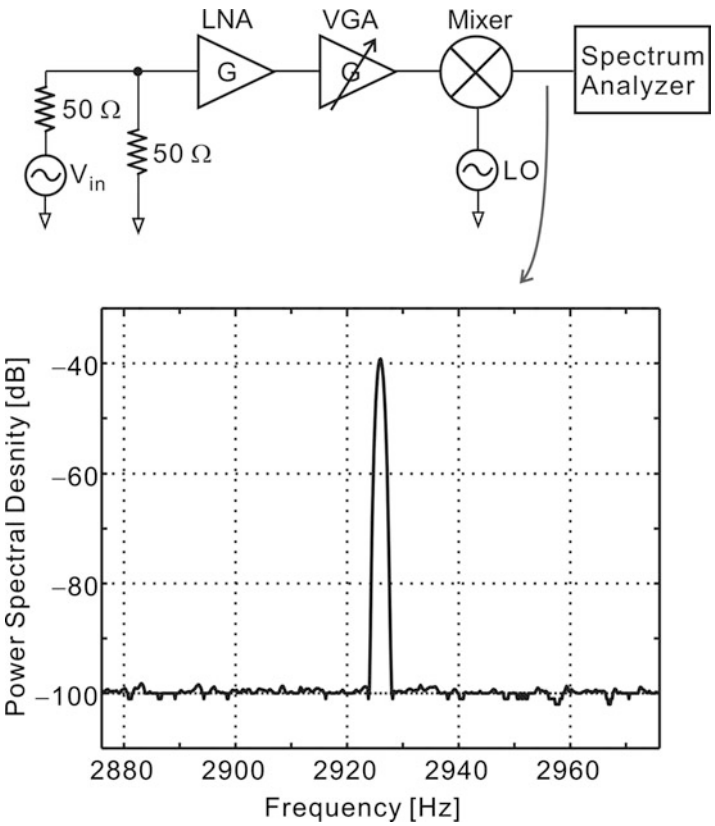

Fig. 8.8 Measured receiver output power spectrum for a -100-dBm, 21-MHz RF signal and with a 21.003-MHz square wave LO

chip, on which an aqueous sample is placed, is left exposed while the rest of the chip is encapsulated.

8.3.1 Receiver Measurement

To measure the receiver input-referred noise, we feed a 100-dBm, 21-MHz RF signal to the receiver's LNA input and use a 21.003-MHz square wave as a local oscillator signal. From the signal and noise power spectrum measured at the receiver's mixer output (Fig. 8.8) using an Agilent E4448 spectrum analyzer, the receiver gain is inferred, and then, by dividing the measured output noise with the gain, the receiver input-referred noise of $1.26\,\mathrm{nV}/\sqrt{Hz}$ is extracted. In this process, the image effect due to the frequency down-conversion is factored

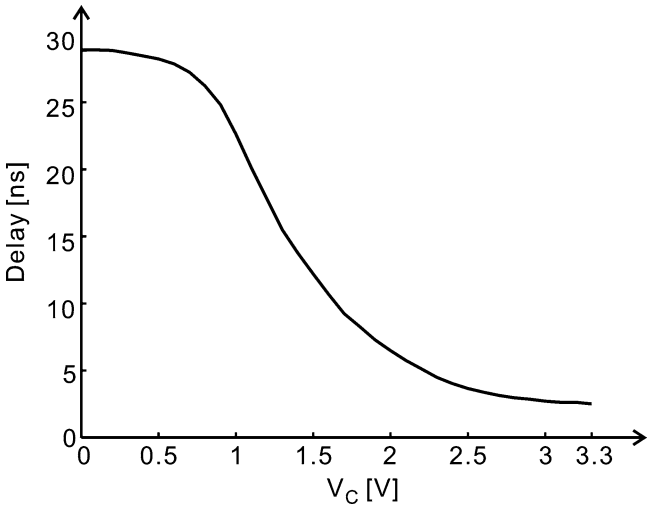

Fig. 8.9 Measured total VCDL delay versus control voltage V_C

out, for the actual operation indeed performs image rejection via back-end digital signal processing (Sect. 8.2.1). Using the measured input-referred noise and the coil impedance (Sect. 8.2.2), we infer the receiver NF. In the palm system, a passive gain of 28 offered by the resonance matching (Sect. 8.2.4) lowers the NF from 22.5 to 0.9 dB. In the 1-chip system, a passive gain of 2.1 lowers the NF from 6.1 to 2.2 dB. The combination of the small input-referred noise and the resonance matching (optimum noise matching) leads to sufficiently low NF, making the ping-pong-ball-sized magnet and the lossy on-chip coil viable system options.

8.3.2 Transmitter Measurements

The measured output impedance of the differential PA (Sect. 8.2.3) is 27. With the power supply V_{DD} of 3.3 V, the maximum deliverable power at the fundamental tone is 82 mW. The measured delay versus control voltage, V_C, of the entire voltage-controlled delay line (VCDL) in the duty cycle controller (Fig. 8.5, bottom left) is shown in Fig. 8.9. The delay is altered from 29 to 2 ns, as V_C is varied from 0 to 3.3 V.

The measured duty cycle as a function of V_C for a 21-MHz excitation signal is shown in Fig. 8.10. As V_C is changed from 0 to 3.3 V, the duty cycle increases from 0 % to 45 %. This translates to the tuning of output power at the fundamental tone from 0 to 80 mW (98 % of the total deliverable power of 82 mW).

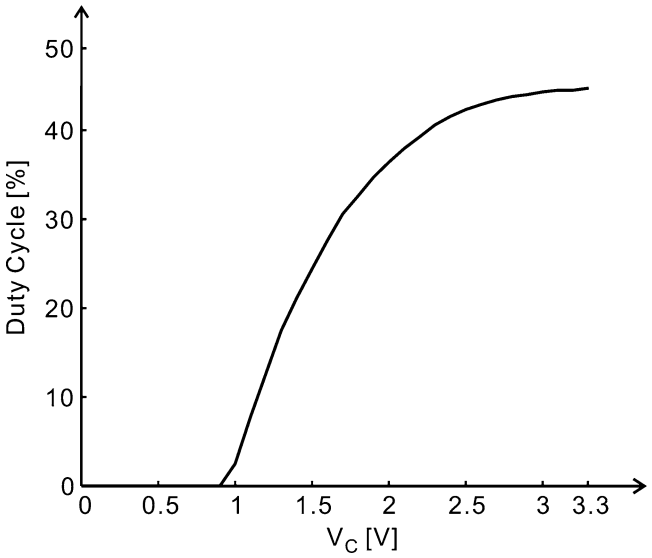

Fig. 8.10 Measured excitation signal duty cycle versus control voltage V_C

8.4 NMR Experiments and NMR-Based Biomolecular Sensing

8.4.1 Proton NMR Experiments

NMR is performed on protons of hydrogen atoms in a 2-μL water sample using the palm system. Figure 8.11 shows a measured, down-converted NMR signal. The repeated ringings, which are the result of the proton excitations using a CPMG pulse sequence [6], constitute the NMR signal. It decays with characteristic time called T_2, one of the key parameters in NMR experiments [6], which we use in our NMR-based biomolecular sensing, as seen shortly. $T_2 = 100$ ms is extracted from the exponentially decaying envelope of the NMR signal, shown as a dotted line. The repeated spikes between the ringings are due to the coupling of the large excitation signals, but they do not compromise the observation of the NMR signal (ringings), as they occur at different time instances. The spin-mass (the minimum mass of water that produces a detectable NMR signal; a smaller minimum mass corresponds to a higher spin-mass sensitivity) sensitivity is 2.5 times higher than that of the 2-kg portable system and 150 times higher than that of the state-of-the-art commercial system [1].

Figure 8.12a shows a measured, down-converted NMR signal obtained in a proton NMR experiment (5 − μL water sample) done with the 1-chip system, from which we obtain $T_2 = 722$ ms. The spikes coupled from the large excitation signals are more pronounced, but once again, they do not hamper the observation

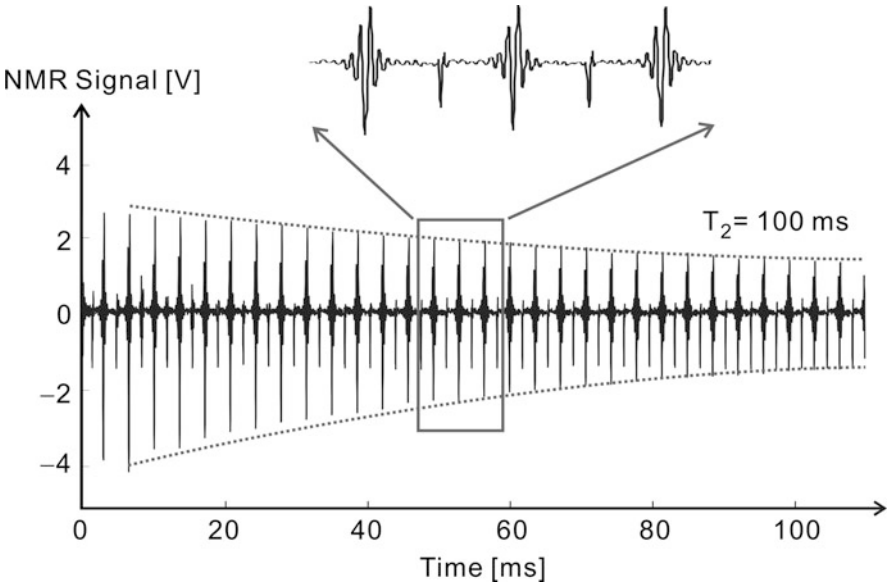

Fig. 8.11 Water proton NMR signal measured with the palm system (From Ref. [3])

of the NMR signal due to their occurrence at different time instances. Note the difference between the values measured using the 1-chip and palm systems. While $T_2 = 722$ ms obtained with the 1-chip system well approximates the true value, $T_2 = 100$ ms obtained with the palm system is a substantial underestimation of the true value, which is due to the pronounced static magnetic field inhomogeneity of the ping-pong-ball-sized magnet used in the palm system [6]. Nonetheless, this is not a fundamental problem, as repetition of the CPMG pulses at a faster rate, which the current implementation has no provision for but is easy to incorporate, can readily yield the correct value [6]. Moreover, in our T_2-based biomolecular sensing experiments that will be presented shortly, we focus on the relative measure of values.

Figure 8.12b shows a measured, down-converted NMR signal obtained in another water proton NMR experiment using the 1-chip system, this time, after 0.05 mM magnetic nanoparticles [Fe] (30 nm) are added in the water sample. The measured T_2 is decreased to 93 ms. This reduction of the T_2 value in the presence of magnetic nanoparticles, which perturb the NMR behavior, is expected from the NMR theory [8].

8.4.2 NMR-Based Biomolecular Sensing

Figure 8.13 shows the detection of avidin protein using the palm system. Magnetic particles (38 nm) coated with biotins are put into a 2−μL water inside the solenoidal

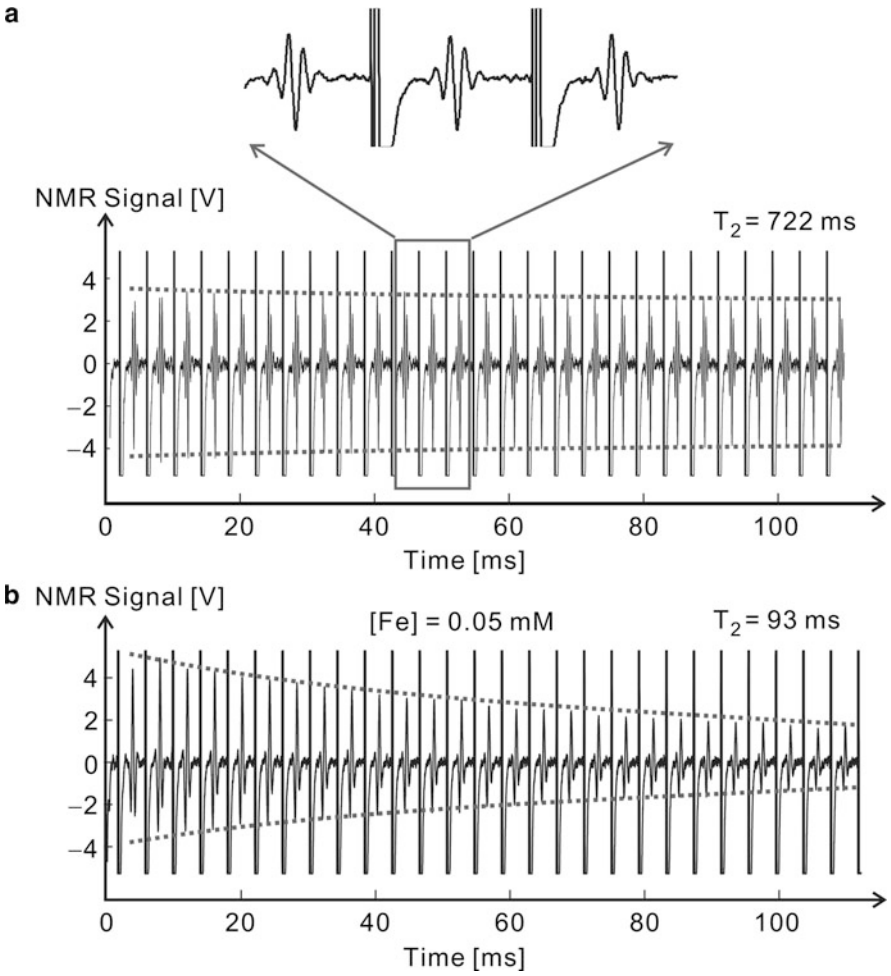

Fig. 8.12 Measured proton NMR signal with the 1-chip system. (**a**) Water. (**b**) Water with magnetic nanoparticles (0.05 mM) (From Ref. [3])

coil. In the absence of avidin (Fig. 8.13, top), the particles stay uniformly dispersed, yielding T_2 of 48 ms. In the presence of avidin (Fig. 8.13, bottom), the biotinylated magnetic particles bind to avidin to self-assemble into clusters [9]. The effectively larger magnetic particles reduce T_2 to 40 ms [9]. The reduction in T_2 corresponds to the detection of avidin. The palm system detects down to 1 avidin molecule in 600 million water molecules.

We use the 1-chip system to detect human chorionic gonadotropin (hCG), the hormonal protein found in blood or urine (Fig. 8.14). Its primary use for female

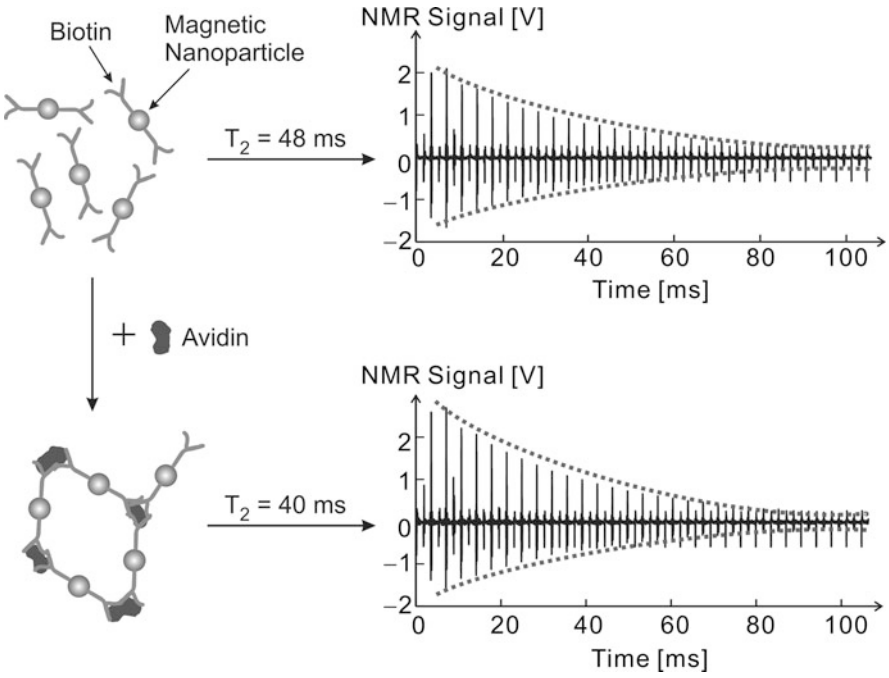

Fig. 8.13 Avidin detection using biotinylated magnetic particles with the palm system (From Ref. [3])

patients is as a pregnancy indicator, but for male patients it serves as a marker for certain cancers, such as choriocarcinoma, germ cell tumors, and islet cell tumors. Magnetic particles (38 nm) coated with mouse monoclonal antibody to hCG are put into a $5-\mu$L water sample placed on the on-chip planar coil. $T_2 = 169$ ms in the absence of hCG, and $T_2 = 141$ ms in its presence, which corresponds to the detection of hCG. The 1-chip system detects down to 1 hCG molecule in 12 billion water molecules.

We also detect human bladder cancer cells using the 1-chip system (Fig. 8.15). Magnetic particles (40 nm) coated with monoclonal antibody to bladder cancer cell surface markers are put into a $5-\mu$L water sample placed on the on-chip coil. In the absence of the cancer cells, the magnetic particles are monodispersed (Fig. 8.15, top left); in the presence of the cancer cells, magnetic particles bind to the cell surface (Fig. 8.15, bottom left). A following centrifugation step [10] separates the cells and unbounded magnetic particles in different layers, and then the unbounded magnetic particles are washed out. As a result, for the sample without cancer cells, all magnetic particles are removed in the washout process, leading to a longer T_2 of 506 ms (Fig. 8.15, top); for the sample with cancer cells, the magnetic particles that bind to the cell surface remain, leading to a shorter T_2 of 440 ms (Fig. 8.15, bottom).

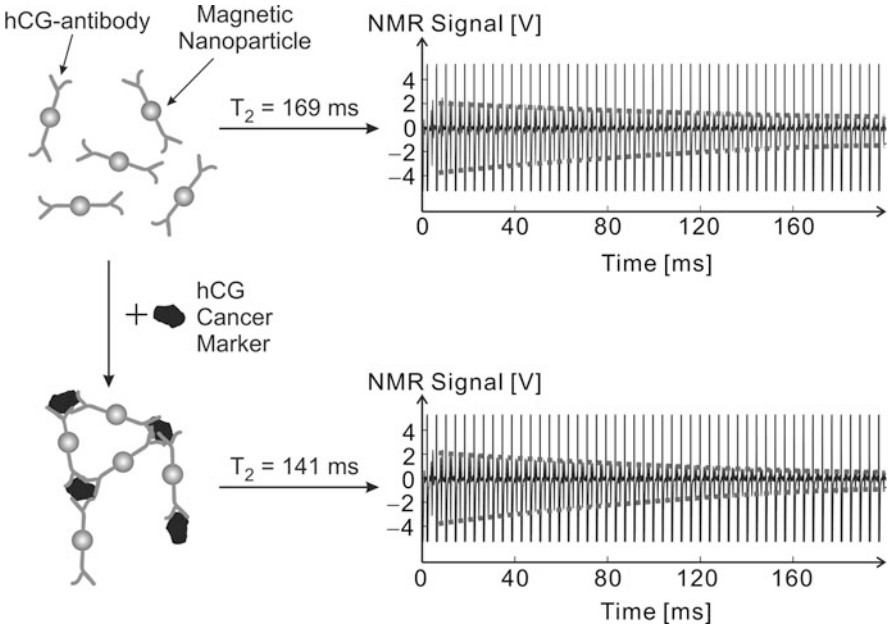

Fig. 8.14 hCG detection with the 1-chip system (From Ref. [3])

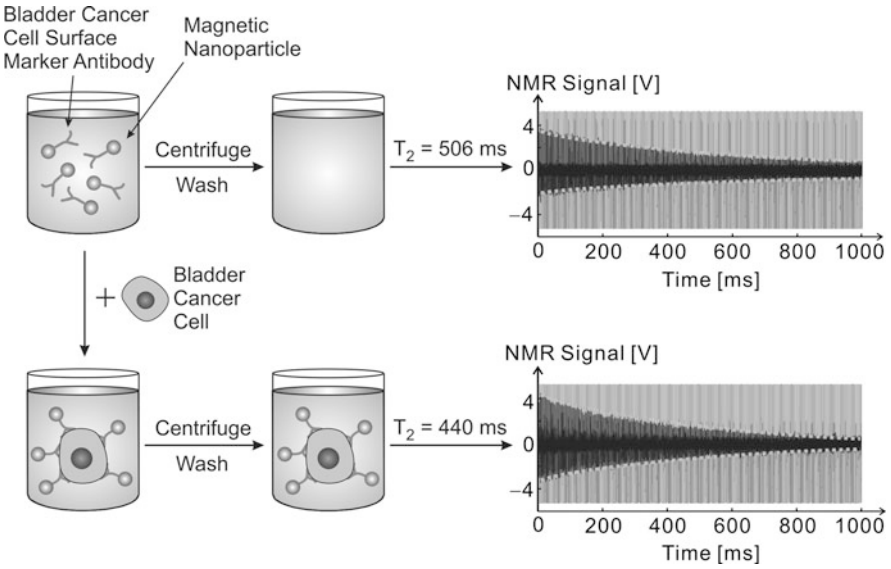

Fig. 8.15 Human bladder cancer cell detection with the 1-chip system (From Ref. [3])

Table 8.1 NMR system miniaturization efforts

	Transceiver integration	Small magnet	On-chip coil
Our 2-kg portable system	O receiver; pulse generator	O 1.25 kg	×
Our palm NMR system	O receiver; transmitter	O 0.07 kg	×
Our 1-chip NMR system	O receiver; transmitter	O 1.25 kg	O
[11]	×	O 1.25 kg	×
[12]	×	O 2.5 kg	×
[13]	O receiver	×	O
[14]	O LNA	×	O
[15]	O LNA	×	×
[16]	O LNA; PA	×	×
[17]	O LNA	×	×

The reduction in T_2 indicates the existence of cancer cells. The concentration detection threshold is 17.5 cells per μL.

8.5 Comparison to Other Miniaturization Works

Before concluding, we compare our miniature NMR systems to other NMR system miniaturization efforts [11–17]. As shown in Table 8.1, other works use small magnets [11, 12] or integrated transceivers [13–17], but not both as we did. In addition, the integrated transceivers used in [13–17] have integration levels considerably lower than ours. Overall, in terms of the entire system dimension and integration level, our miniature NMR systems represent a meaningful advance from previous miniaturization efforts.

8.6 Conclusion

By combining the physics of NMR with silicon RF integrated circuits, we developed three miniature NMR systems for biomolecular sensing ultimately aimed at disease screening. We would like to view the value of our work from a few different angles. First, NMR has a broad array of applications in addition to biomolecular sensing, and from this general NMR point of view, our work on the small, low-cost NMR is a meaningful development that can help make the benefits of NMR closer to our lives. Second, from the circuit point of view, our work showcases how silicon RF integrated circuits can be used not only for wireless applications but also in 1 day for human health care and disease screening in direct interface with biological systems. Third, from the biotechnology point of view, our work suggests a way to perform general-purpose disease screening in the low-cost, handheld platform.

References

1. Bruker Optics. *The Minispec TD-NMR Analyzers*. (Bruker Optics, Billerica) [Online]. Available: http://www.brukeroptics.com/minispec.html (2012)
2. N. Sun, Y. Liu, H. Lee, R. Weissleder, and D. Ham, CMOS RF biosensor utilizing nuclear magnetic resonance, IEEE J. Solid-State Circ. **44**(5), 1629–1643, (2009)
3. N. Sun, T.-J. Yoon, H. Lee, W. Andress, R. Weissleder, D. Ham, Palm NMR and one-chip NMR.IEEE J. Solid-State Circ. **46**(1), 342–352 (2011)
4. B. Sun and K.-J. Dunn,A global inversion method for multi-dimensional NMR logging, J. Magn Reson 172, 152–160, (2005).
5. L.M.K. Vandersypen, M. Steffen, G. Breytal, C. S. Yannoni, M. H. Sherwood, I.L. Chuang, Experimental realization of Shor's quantum factoring algorithm using nuclear magnetic resonance, Nature, **414**, 883–887 (2001)
6. C.P. Slichter, *Principles of Magnetic Resonance* Springer,New York, 1992.
7. T.H. Lee, *The Design of CMOS Radio-Frequency Integrated Circuits*. Cambridge University Press, Cambridge, UK 1998.
8. A. Roch, R.N. Muller, and P. Gillis, Theory of proton relaxation induced by superparamagnetic particles, J. Chem Phys **110**(11), 5403–5411 (1999)
9. J.M. Perez, L. Josephson, T. O'Loughlin, D. Hoegeman, R.Weissleder, Magnetic relaxation switches capable of sensing molecular interactions, Nat Biotechnol. **20**, 816–820 (2002)
10. H. Lee, T.-J. Yoon, J.-L. Figueiredo, F. K. Swirski, R.Weissleder, Rapid detection and profiling of cancer cells in fine-needle aspirates, *Proc. Natl. Acad. Sci* **106**(30), 12459–12464 (2009)
11. H. Lee, E. Sun, D. Ham, R.Weissleder, Chip-NMR biosensor for detection and molecular analysis of cells, Nat Med **14**(8), 869–874, (2008)
12. G. Eidmann, R. Savelsberg, P. Blümler, B. Blümich, The NMR mouse, a mobile universal surface explorer,J. Magn Reson **122**, 104–109 (1996)
13. G. Boero, J. Frounchi, B. Furrer, P.-A. Besse, R.S. Popovic, Fully integrated probe for proton nuclear magnetic resonance magnetometry, Rev Sci Instrum. 72, 2764–2768, (2001).
14. J. Anders, G. Chiaramonte, P. SanGiorgio, G. Boero, A.singlechip array of NMR receivers, J. Magn Reson. **201**, 239–249 (2009)
15. T. Cherifi, N. Abouchi, G.-N. Lu, L. Bouchet-Fakri, L. Quiquerez, B. Sorli, J.-F. Chateaux, M. Pitaval, P. Morin, A CMOS microcoil-associated preamplifier for NMR spectroscopy, in *IEEE Transactions on Circuits and Systems I, Regular Papers*, vol. 52, no. 12(2005) pp. 2576–2583,
16. L.-S. Fan, S. Hsu, J.-D. Jin, C.-V. Hsieh, W.-C. Lin, H. Hao, H.-L. Cheng, K.-C. Hsueh, and C.-Z. Lee, Miniaturization of magnetic resonance microsystem components for 3D cell imaging, in *IEEE International Solid-State Circuits Conference Digest of Technical Papers* (2007), pp.166–167, San Francisco, CA.
17. R.L. Magin, A.G. Webb, and T.L. Peck, Miniature magnetic resonance machines,IEEE Spect **34**(10), 51 (1997)